Journal Européen des Systèmes Automatisés
Vol. 58, No. 1, January, 2025, pp. 75-87
Journal homepage: http://iieta.org/journals/jesa

# Eliminating Chattering in Prosthetic Fingers Using Classic Synergetic Control

Aya Khudhair Abbas, Saleem Khalefa Kadhim*

Department of Control and System Engineering, University of Technology-Iraq, Baghdad 10066, Iraq

Corresponding Author Email: Saleem.K.Kadhim@uotechnology.edu.iq



https://doi.org/10.18280/jesa.580109

**Received:** 28 July 2024
**Revised:** 29 September 2024
**Accepted:** 10 October 2024
**Available online:** 31 January 2025

***Keywords:***
*prosthetic fingers, finger amputations, chattering effect, classic synergetic control (CSC), controlling prosthetic fingers, desired phalange position*

**ABSTRACT**

Prosthetic fingers are advancing to help individuals with amputations because of congenital deformities, infections, or accidents have a significant impact on their ability to perform daily tasks as well as their self-confidence. with improved gripping capabilities and natural movement, but controlling them and mitigating chattering remain challenging. To address this, a classic synergetic controller (CSC) was developed using mathematical formulas to control the joint angle position of the Prosthetic finger and accomplish accurate tracking. demonstrating superior performance over Classical Sliding Mode (CSMC) control by 20% in efficiency and robustness. The CSC enabled the prosthetic finger to reach and maintain the desired position angle in 9 seconds without chatter and successfully eliminated chattering under uncertainty, a previously unaddressed issue in prosthetic finger control. The CSC system provided global stability and flexibility in responding to parameter changes, allowing for precise tracking of the finger's movement. These encouraging findings point to a major impact on upcoming developments in the production of prosthetic fingers, opening up new possibilities for use.

## 1. INTRODUCTION

A prosthetic finger is a custom-made device to replace a missing or dysfunctional finger, restoring function and appearance [1]. It can range from simple cosmetic covers to advanced robotic prostheses with sophisticated functionalities [2]. Advancements in materials science, biomechanics, and prosthetic technology have led to sophisticated prosthetic fingers using materials like silicone, carbon fiber, and lightweight metals, though challenges such as size, weight, and stiffness complicate controller design and accurate mathematical modeling; advanced prosthetics often incorporate electronics, sensors, and microprocessors to enable natural movement and precise control [3]. Several studies have shown that prosthetic fingers significantly improve hand function and psychosocial well-being, highlighting their importance in enhancing the quality of life for individuals with finger amputations [4-7]. Scholars have proposed various feasible control strategies for prosthetic finger control, and past researchers have utilized different approaches in MATLAB simulations.

Despite significant advancements in control strategies for prosthetic fingers, effectively controlling of prosthetic fingers and mitigating the chattering effect inherent in robust methods like Sliding Mode Control (SMC) and Adaptive Sliding Mode Control (ASMC) remains challenging. Existing approaches, such as Proportional Integral Derivative (PID), Fuzzy Logic Control (FLC), and computed torque control, have benefits and limitations but do not fully address chattering or the complexities of nonlinear systems and input uncertainties, necessitating further research for robust, stable, and precise control strategies.

Arslan et al. [2, 4] compared the path-tracking efficiency of various control strategies, including FL, SMC, and PID controllers. They evaluated these different strategies using a biomimetic robot hand-finger model, analyzing simulation results quantitatively. They found that caution is needed when interpreting these findings as they are based on simulations rather than real-world applications. Therefore, the study emphasized the analysis of experimental results, including tendon forces and prosthetic finger motion.

Xu et al. [8] presented findings from a project using two synergistic inputs to achieve precise movements with a prosthetic hand. They established postural synergy on a phantom hand, kinematically identical to a real hand, to better replicate intended poses for manipulation tasks. They developed and assembled the prosthetic hand, qualitatively verifying its motion ranges. This technique allows imaginary hand positions to be accurately replicated by the prosthetic hand using contralateral postural synergies and synergistic inputs, enabling continuous transition between positions.

Lysenko et al. [9] proposed a mathematical model for a biomechanical finger prosthesis, focusing on its dynamics during a broader range of movements. They concluded that the control system's mathematical model was accurately constructed, ensuring regulator output values stayed within permissible limits and control time closely matched the engine's constant time.

Hamidi et al. [10] introduced classical and adaptive control designs based on synergetic theory for tracking control of a single-link robot arm actuated by artificial muscles. The ASMC addresses uncertainties in muscle parameters and

ensures system stability. Simulated results indicate that the optimized control design provides superior tracking performance in terms of transient and steady-state characteristics compared to non-optimal designs, despite higher power consumption. In the presence of parameter uncertainties, the adaptive control system outperforms non-adaptive systems.

Al-Hussein et al. [11] studied the suppression of chaotic oscillations in a three-conductor power system. They utilized an ASMC algorithm along with a Static Synchronous Compensator (STATCOM) and energy storage devices in their control unit design. The system's dynamics displayed critical chaotic oscillations influenced by specific parameters, which can jeopardize power system bus voltage stability. Chaos in power systems may lead to system collapse, significantly impacting the quality of commercial power services.

The Shadow Robot Company [12] created the Shadow Dexterous Hand, a humanoid robotic hand system with 24 movements that closely resembles the dexterity and kinematics of a human hand. PID controllers are configured during setup, and control strategies are implemented via EtherCAT. Depending on the launch file selected, software testing on both simulated and real hardware can be done seamlessly using the same interface thanks to the drivers provided by the shadow robot EtherCAT stack and a simulated hand model available in the Gazebo simulator.

Fan et al. [13] suggested an adaptive grasp technique that uses error estimation compensation and collaboration control to mitigate object pose uncertainty. The error compensation method estimates the object's pose error based on finger tactile information and uses multiple techniques to compensate for it based on different error ranges. The outcomes demonstrate that this adaptive grasp strategy greatly raises the success rate of grasping objects in uncertain poses.

Li et al. [14] proposed a new object-level impedance control framework aimed at improving grasp force and quality. By dynamically sliding from the initial to the final grasp configuration, optimal grasp quality is achieved. The proposed controller allows the object to be maneuvered in hand while responding to external forces. Proper design parameter selection, as verified by a Lyapunov function, ensured the closed-loop robotic system's effective control performance.

Shahriari et al. [15] developed a single-arm control policy that applies to all robots in a multi-manual system, including an adaptive force-impedance controller based on a modeled control objective. Two experiments were carried out: the first involved a bi-manual system grasping and moving an object along a desired path, and the second tested a teleoperation setup that allowed remote control of the object. The findings demonstrated the approach's robustness and practicability.

Zhang et al. [16] proposed adaptive sliding mode friction indemnification adaptive impedance controllers for a stereophonic artificial hand. To satisfy the demands of a force-tracking impedance controller, they created a five-fingered hand with multisensory abilities and DSP-based control hardware and software. According to experimental results, in uncertain environments with unknown stiffness and position, the adaptive controller with friction indemnification was able to achieve accurate force-tracking and stable torque/force response.

Jalani et al. [17] offered a novel approach to active compliance control using Integral Sliding Mode Control (ISMC), which combines a virtual mass-spring damper for compliant control with a model reference approach. The task controller demonstrated excellent tracking performance in spite of high friction and stiction, according to the results. Furthermore, by using the posture controller for the index and thumb fingers in conjunction with spherical and cylindrical coordinates, the fingers were able to move around the object without colliding, highlighting the grasping task.

Herrmann et al. [18] proposed a new approach to using ISMC for active compliance control. The use of spherical and cylindrical coordinates, combined with the posture controller for the thumb and index finger, ensured that both fingers moved around the object without colliding, allowing for practical and powerful grasping. Furthermore, BERUL fingers with tactile pressure sensors reduced the force applied to objects. An automated tuning procedure demonstrated the effectiveness of this compliant control in grasping similar objects at various required force levels.

Labbadi and Cherkaoui [19] examined a robust, adaptive controller for tracking and stabilizing the flight path of quadrotor Unmanned Aerial Vehicles (UAVs). They used the Newton-Euler method to determine the dynamics of the quadrotor and created two sturdy controllers to control parametric uncertainties. This design combines SMC methods with the Adaptive Backstepping approach.

Mohd Zaihidee et al. [20] investigated cutting-edge SMC applications for permanent magnet synchronous motor (PMSM) speed control. The study identified several areas that require additional research, such as the application of sliding mode observers in conjunction with other controllers, SMC for PMSM Direct Torque Control (DTC), and sensorless speed control applications utilizing sliding mode controllers.

A neuro-sliding mode control approach was tested using a reference compensation technique in a non-model-based control framework [21]. A Radial Basis Function (RBF) network, similar to a Multi-Layer Perceptron (MLP), was used to account for uncertainties in a three-link robot manipulator. A stability analysis of the neuro-sliding mode control scheme was carried out, and simulation results showed that it outperformed traditional sliding mode control in tracking performance.

Majeed et al. [22] focused on modeling and controlling a tendon-driven prosthetic finger resembling a human index finger. They employed CSMC and ASMC techniques to manage finger movements, aiming to overcome CSMC's chatter issue. Their findings demonstrated that ASMC outperformed CSMC, offering quicker response times and reduced chatter during prosthetic finger movements.

Analysis of existing literature identified a gap in controlling of prosthetic fingers, which poses greater challenges than fully actuated ones. Many existing control strategies, including PID, FLC, and computed torque control, have limitations that prevent them from fully addressing the complexities and issues such as the chattering effect and system uncertainties, necessitating further research for more robust solutions.

Previous studies have not investigated the use of CSC in prosthetic finger motion, despite its potential to improve stability and reduce chattering, which could otherwise damage the prosthetic finger. Research on CSC specifically for prosthetic finger control is lacking. Where the CSC offers several advantages: it provides robust control against disturbances and parameter variations, enables precise regulation of system states, manages nonlinear dynamics effectively, maintains system stability in dynamic environments, and can be adapted to various system

configurations.

Therefore, this paper proposes a novel anti-interference control strategy for trajectory tracking in the joint space of a grasp-driven prosthetic finger. It integrates CSC to enhance stability and eliminate chattering during finger motion, aiming to prevent potential damage to the prosthetic finger. Wherefore, this work presents a CSC to control the variables of a constrained prosthetic finger, aiming to maintain system robustness amid parameter variations and disturbances. Also, it involves analyzing the dynamic model and state space representation of the robotic manipulator, developing CSC algorithms, and conducting stability analysis based on the control law to ensure consistent and stable motion of the manipulator.

The primary advantages of the CSC approach include:

- CSC offers robust control against parameter variations, ensuring stable performance without chattering in dynamic and uncertain environments.
- CSC algorithms enable precise regulation of system states, which is essential for controlling complex and underactuated robotic systems.
- CSC efficiently manages nonlinear dynamics, making it ideal for systems with complex interactions and constraints.
- CSC contributes to system stability by analyzing the dynamic model and state-space representations.
- Designing rules for CSC is based on straightforward mathematical principles, making it simple to implement even in complex systems.
- CSC can be customized to meet specific system configurations and requirements, increasing its applicability across a wide range of robotic systems and manipulations.

This paper will include the following sections, in sequential order:

- The dynamics and control model outlines the mathematical model of a prosthetic finger actuated by CSC.
- Results and Discussion Show simulation results and discuss the control system and model response.
- Finally, the paper is concluded with a section titled Conclusion. The methodology of this paper is described in the block diagram shown in Figure 1, which depicts the sequence of presenting the contents of this research.

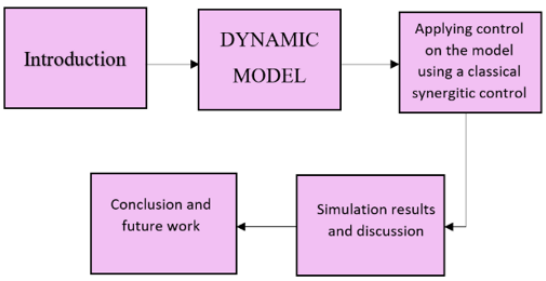


**Figure 1.** Block diagram of the methodology

## 2. DYNAMICS MODEL

Advancements in robotic hands have greatly enhanced productivity and efficiency in the automation industry, where robots perform a range of tasks including cutting, welding, assembling, and picking and placing [23]. Figure 2 shows the structure of a prosthetic finger hand driven by an index finger. A prosthetic finger consists of three phalanges that correspond to the middle, proximal, and distal bones of the index finger [24, 25]. Every degree of freedom of the prosthetic finger is driven by a motor conveyor belt. Through the bully, the motor, which is mounted on the forearm frame, drives phalanges to give a pull control.

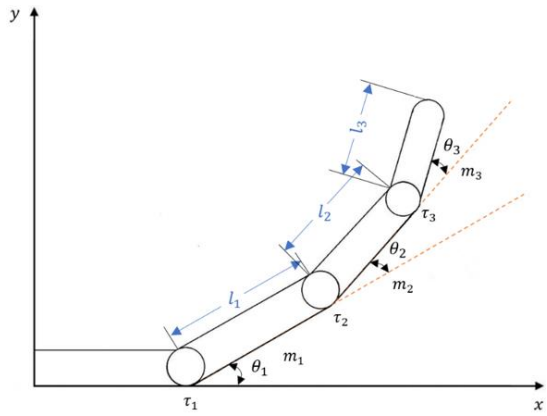


**Figure 2.** Schematic diagram for the three phalanges finger

In tendon-driven finger movement, power from the motor to the joint is transferred via a belt, where the belt's flexibility primarily affects the joint, akin to a flexible joint. The analysis employs Lagrangian formulation to derive the equation of motion. The mathematical expression for the Lagrangian equation is articulated as follows [26, 27]:

$$L = KE - PE \tag{1}$$

where, *KE* is the kinetic energy, and *PE* represents is the potential energy.

$$\begin{aligned} L = {} & [0.5(m_1 + m_2 + m_3)l_1^2 + 0.5(m_2 + m_3)l_2^2 \\ & +(m_2 + m_3)l_1 l_2 \cos\theta_2 + 0.5m_3 l_3^2 \\ & +m_3 l_1 l_3 \cos(\theta_2 + \theta_3) + m_3 l_2 l_3 \cos\theta_3]\dot{\theta}_1^2 \\ & +[0.5(m_2 + m_3)l_2^2 + 0.5m_3 l_3^2 + m_3 l_2 l_3 \cos\theta_3]\dot{\theta}_2^2 \\ & +[0.5m_3 l_3^2]\dot{\theta}_3^2 \\ & +[(m_2 + m_3)l_1 l_2 \cos\theta_2 + (m_2 + m_3)l_2^2 \\ & +m_3 l_3^2 + m_3 l_1 l_3 \cos(\theta_2 + \theta_3) \\ & +2m_3 l_2 l_3 \cos\theta_3]\dot{\theta}_1\dot{\theta}_2 \\ & +\begin{bmatrix} m_3 l_3^2 + m_3 l_1 l_3 \cos(\theta_2 + \theta_3) \\ +m_3 l_2 l_3 \cos\theta_3 \end{bmatrix}\dot{\theta}_1\dot{\theta}_3 \\ & +[m_3 l_3^2 + m_3 l_2 l_3 \cos\theta_3]\dot{\theta}_2\dot{\theta}_3 \\ & -(m_1 + m_2 + m_3)g l_1 \sin\theta_1 \\ & -(m_2 + m_3)g l_2 \sin(\theta_1 + \theta_2) \\ & -m_3 g l_3 \sin(\theta_1 + \theta_2 + \theta_3) \end{aligned} \tag{2}$$

The Lagrange-Euler method can be used to derive the dynamic model of a 3-DoF cable-driven prosthetic finger, the equations of motion for each phalanx coordinate $\theta_1$, $\theta_2$, and $\theta_3$ can be derived, providing the applied torque on each joint as follows:

$$\left.\frac{d}{dt}\left[\frac{\partial L}{\partial \dot{\theta}_i}\right] - \frac{\partial L}{\partial \theta_i} = \tau_i\right\} \tag{3}$$

where, τ is the torque applied to each joint in the system and $i$=1,2,3

$$
\begin{aligned}
&[(m_1+m_2+m_3)l_1^2+(m_2+m_3)l_2^2+m_3l_3^2\\
&\quad+2m_2l_1l_2\cos\theta_2\\
&\quad+2m_3l_1l_2\cos\theta_2\\
&\quad+2m_3l_1l_3\cos(\theta_2+\theta_3)\\
&\quad+2m_3l_2l_3\cos\theta_3]\ddot{\theta}_1\\
&\quad+[m_2l_1l_2\cos\theta_2+m_3l_1l_2\cos\theta_2\\
&\quad+m_2l_2^2+m_3l_2^2+m_3l_3^2\\
&\quad+m_3l_1l_3\cos(\theta_2+\theta_3)\\
&\quad+2m_3l_2l_3\cos\theta_3]\ddot{\theta}_2\\
&\quad+[m_3l_3^2+m_3l_1l_3\cos(\theta_2+\theta_3)\\
&\quad+m_3l_2l_3\cos\theta_3]\ddot{\theta}_3\\
&\quad-[2m_2l_1l_2\sin\theta_2\\
&\quad+2m_3l_1l_2\sin\theta_2\\
&\quad+2m_3l_1l_3\sin(\theta_2+\theta_3)]\dot{\theta}_1\dot{\theta}_2\\
&\quad-[2m_3l_1l_3\sin(\theta_2+\theta_3)\\
&\quad+2m_3l_2l_3\sin\theta_3]\dot{\theta}_1\dot{\theta}_3\\
&\quad-[2m_3l_1l_3\sin(\theta_2+\theta_3)\\
&\quad+2m_3l_2l_3\sin\theta_3]\dot{\theta}_2\dot{\theta}_3\\
&\quad-[m_2l_1l_2\sin\theta_2+m_3l_1l_2\sin\theta_2\\
&\quad+m_3l_1l_3\sin(\theta_2+\theta_3)]\dot{\theta}_2^2\\
&\quad-[m_3l_1l_3\sin(\theta_2+\theta_3)\\
&\quad+m_3l_2l_3\sin\theta_3]\dot{\theta}_3^2\\
&\quad+(m_1+m_2+m_3)gl_1\cos\theta_1\\
&\quad+(m_2+m_3)gl_2\cos(\theta_1+\theta_2)\\
&\quad+m_3gl_3\cos(\theta_1+\theta_2+\theta_3)=\tau_1
\end{aligned}
\tag{4}
$$

$$
\begin{aligned}
&[(m_2+m_3)l_1l_2\cos\theta_2+(m_2+m_3)l_2^2+m_3l_3^2\\
&\quad+m_3l_1l_3\cos(\theta_2+\theta_3)\\
&\quad+2m_3l_2l_3\cos\theta_3]\ddot{\theta}_1\\
&\quad+[(m_2+m_3)l_2^2+m_3l_3^2\\
&\quad+2m_3l_2l_3\cos\theta_3]\ddot{\theta}_2\\
&\quad+[m_3l_3^2+m_3l_2l_3\cos\theta_3]\ddot{\theta}_3\\
&\quad-[2m_3l_2l_3\sin\theta_3]\dot{\theta}_1\dot{\theta}_3\\
&\quad-[2m_3l_2l_3\sin\theta_3]\dot{\theta}_2\dot{\theta}_3\\
&\quad+[(m_2+m_3)l_1l_2\sin\theta_2\\
&\quad+m_3l_1l_3\sin(\theta_2+\theta_3)]\dot{\theta}_1^2\\
&\quad-[m_3l_2l_3\sin\theta_3]\dot{\theta}_3^2\\
&\quad+(m_2+m_3)gl_2\cos(\theta_1+\theta_2)\\
&\quad+m_3gl_3\cos(\theta_1+\theta_2+\theta_3)=\tau_2
\end{aligned}
\tag{5}
$$

$$
\begin{aligned}
&[m_3l_3^2+m_3l_1l_3\cos(\theta_2+\theta_3)+m_3l_2l_3\cos\theta_3]\ddot{\theta}_1\\
&\quad+[m_3l_3^2+m_3l_2l_3\cos\theta_3]\ddot{\theta}_2\\
&\quad+[m_3l_3^2]\ddot{\theta}_3\\
&\quad+[2m_3l_2l_3\sin\theta_3]\dot{\theta}_1\dot{\theta}_2\\
&\quad+[m_3l_1l_3\sin(\theta_2+\theta_3)\\
&\quad+m_3l_2l_3\sin\theta_3]\dot{\theta}_1^2\\
&\quad+[m_3l_2l_3\sin\theta_3]\dot{\theta}_2^2\\
&\quad+m_3gl_3\cos(\theta_1+\theta_2+\theta_3)=\tau_3
\end{aligned}
\tag{6}
$$

$\tau_1$, $\tau_2$, and $\tau_3$ represent the torque at the first, second, and third phalanges respectively, also, $\ddot{\theta}$ is the angular acceleration, it can be expressed in the equations below:

$$M(\theta)\ddot{\theta}+C(\theta,\dot{\theta})\dot{\theta}+G(\theta)=\tau \tag{7}$$

where, $M(\theta)$ is the inertia matrix of the links, $\tau$ represents the control torque, $C\ (\theta,\dot{\theta})\ \dot{\theta}$ is the Coriolis force, and $G(\theta)$ signifies gravitational force. It can be described as Eq. (8):

$$
\begin{bmatrix} M_{11} & M_{12} & M_{13}\\ M_{21} & M_{22} & M_{23}\\ M_{31} & M_{32} & M_{33}\end{bmatrix}\begin{bmatrix}\ddot{\theta}_1\\ \ddot{\theta}_2\\ \ddot{\theta}_2\end{bmatrix}+\begin{bmatrix} C_1\\ C_2\\ C_3\end{bmatrix}\begin{bmatrix}\dot{\theta}_1\\ \dot{\theta}_2\\ \dot{\theta}_3\end{bmatrix}+\begin{bmatrix} G_1\\ G_2\\ G_3\end{bmatrix}=\begin{bmatrix}\tau_1\\ \tau_2\\ \tau_3\end{bmatrix} \tag{8}
$$

$$\tau_1=M_{11}\ddot{\theta}_1+M_{12}\ddot{\theta}_2+M_{13}\ddot{\theta}_3+C_1\dot{\theta}_1+G_1 \tag{9}$$

$$\tau_2=M_{21}\ddot{\theta}_1+M_{22}\ddot{\theta}_2+M_{23}\ddot{\theta}_3+C_2\dot{\theta}_2+G_2 \tag{10}$$

$$\tau_3=M_{31}\ddot{\theta}_1+M_{32}\ddot{\theta}_2+M_{33}\ddot{\theta}_3+C_3\dot{\theta}_3+G_3 \tag{11}$$

$\ddot{\theta}_1, \ddot{\theta}_2$ and $\ddot{\theta}_3$ are:

$$\ddot{\theta}_1=\frac{1}{M_{11}}\left(\tau_1-M_{12}\ddot{\theta}_2-M_{13}\ddot{\theta}_3-C_1\dot{\theta}_1-G_1\right) \tag{12}$$

$$\ddot{\theta}_2=\frac{1}{M_{22}}\left(\tau_2-M_{21}\ddot{\theta}_1-M_{23}\ddot{\theta}_3-C_2\dot{\theta}_2-G_2\right) \tag{13}$$

$$\ddot{\theta}_3=\frac{1}{M_{33}}\left(\tau_3-M_{31}\ddot{\theta}_1-M_{32}\ddot{\theta}_2-C_3\dot{\theta}_3-G_3\right) \tag{14}$$

Selecting a state variable for the state equation can be represented as follows [28, 29]:

$x_1=\theta_1\ x_3=\theta_2\ x_5=\theta_3$ (Angular position of the phalanges)

$x_2=\dot{\theta}_1\ x_4=\dot{\theta}_2\ x_6=\dot{\theta}_3$ (Angular velocity of the phalanges)

Eqs. (15)-(20) highlights the highly nonlinear dynamics of the prosthetic finger. By selecting appropriate state variables in the state equation [30, 31], it can be expressed as follows:

$$\dot{x_1}=\dot{\theta}_1=x_2 \tag{15}$$

$$\dot{x_2}=\ddot{\theta}_1=\frac{1}{M_{11}}\left(\tau_1-M_{12}\ddot{\theta}_2-M_{13}\ddot{\theta}_3-C_1\dot{\theta}_1-G_1\right) \tag{16}$$

$$\dot{x_3}=\dot{\theta}_2=x_4 \tag{17}$$

$$\dot{x_4}=\ddot{\theta}_2=\frac{1}{M_{22}}\left(\tau_2-M_{21}\ddot{\theta}_1-M_{23}\ddot{\theta}_3-C_2\dot{\theta}_2-G_2\right) \tag{18}$$

$$\dot{x_5}=\dot{\theta}_3=x_6 \tag{19}$$

$$\dot{x_6}=\ddot{\theta}_3=\frac{1}{M_{33}}\left(\tau_3-M_{31}\ddot{\theta}_1-M_{32}\ddot{\theta}_2-C_3\dot{\theta}_3-G_3\right) \tag{20}$$

$u_1=\tau_1$ (First phalangeal actuator's torque)
$u_2=\tau_2$ (Second phalangeal actuator's torque)
$u_3=\tau_3$ (Third phalangeal actuator's torque)

## 3. CLASSIC SYNERGETIC CONTROL (CSC) ALGORITHM

Current control theory faces difficulties in addressing the complexity of intricate macro-systems, which involve multi-dimensional, nonlinear dynamics and interconnected subsystems exchanging information, matter, and power. This complexity makes it challenging to identify universal control laws for system synthesis [32]. Comprehensive CSC is an approach designed to manage nonlinear systems by integrating multiple control mechanisms to ensure stability and resilience

despite uncertainties and nonlinearities. This offers a solution for inherently unstable systems [33]. A control strategy has been developed to track the angular position in a prosthetic finger system using the CSC approach to create the CSC algorithm for a prosthetic finger system, following specific steps and assuming no external disturbances [34].

The first step in the design is to define the error $e_1$ is the difference between the desired angle position ($x_{1d}$=$\theta_{1d}$) and the actual angle position ($x_1 = \theta_1$) [35].

$$e_1 = x_1 - x_{1d} \tag{21}$$

$$e_2 = x_3 - x_{3d} \tag{22}$$

$$e_3 = x_5 - x_{5d} \tag{23}$$

$e_2$ is the difference between the desired angle position ($x_{3d}$ =$\theta_{2d}$) and the actual angle position ($x_3 = \theta_2$) and $e_3$ is the difference between the desired angle position ($x_{5d}$ =$\theta_{3d}$) and the actual angle position ($x_5 = \theta_3$).

By calculating the first, second and third derivatives, one can obtain the desired outcome.

$$\dot{e_1} = \dot{x_1} - \dot{x_{1d}} = x_2 - \dot{x_{1d}} \tag{24}$$

$$\dot{e_2} = \dot{x_3} - \dot{x_{3d}} = x_4 - \dot{x_{3d}} \tag{25}$$

$$\dot{e_3} = \dot{x_5} - \dot{x_{5d}} = x_6 - \dot{x_{5d}} \tag{26}$$

$$\begin{aligned}\ddot{e_1} = \dot{x_2} - \ddot{x_{1d}} = \frac{1}{y}[&(M_{22}M_{33} - M_{32}M_{23})u_1 \\ &+ (M_{32}M_{13} - M_{12}M_{33})u_2 \\ &+ (M_{12}M_{23} - M_{22}M_{13})u_3 \\ &+ (M_{32}M_{23} - M_{22}M_{33})C_1 \\ &+ (M_{32}M_{23} - M_{22}M_{33})G_1 \\ &+ (M_{12}M_{33} - M_{13}M_{33})C_2 \\ &+ (M_{12}M_{33} - M_{13}M_{32})G_2 \\ &+ (M_{22}M_{13} - M_{12}M_{23})C_3 \\ &+ (M_{22}M_{13} - M_{12}M_{23})G_3] - \ddot{x_{1d}}\end{aligned} \tag{27}$$

$$\begin{aligned}\ddot{e_2} = \dot{x_4} - \ddot{x_{3d}} = \frac{1}{y}[&(M_{31}M_{23} - M_{21}M_{33})u_1 \\ &+ (M_{11}M_{33} - M_{13}M_{31})u_2 \\ &+ (M_{13}M_{23} - M_{11}M_{23})u_3 \\ &+ (M_{21}M_{33} - M_{31}M_{23})C_1 \\ &+ (M_{21}M_{33} - M_{31}M_{23})G_1 \\ &+ (M_{13}M_{31} - M_{11}M_{33})C_2 \\ &+ (M_{13}M_{31} - M_{11}M_{33})G_2 \\ &+ (M_{11}M_{23} - M_{21}M_{13})C_3 \\ &+ (M_{11}M_{23} - M_{21}M_{13})G_3] - \ddot{x_{3d}}\end{aligned} \tag{28}$$

$$\begin{aligned}\ddot{e_3} = \dot{x_6} - \ddot{x_{5d}} = \frac{1}{y}[&(M_{32}M_{21} - M_{31}M_{22})u_1 \\ &+ (M_{31}M_{12} - M_{32}M_{11})u_2 \\ &+ (M_{11}M_{22} - M_{21}M_{12})u_3 \\ &+ (M_{31}M_{22} - M_{32}M_{21})C_1 \\ &+ (M_{31}M_{22} - M_{32}M_{21})G_1 \\ &+ (M_{32}M_{11} - M_{31}M_{12})C_2 \\ &+ (M_{32}M_{11} - M_{31}M_{12})G_2 \\ &+ (M_{21}M_{12} - M_{11}M_{22})C_3 \\ &+ (M_{21}M_{12} - M_{11}M_{22})G_3] - \ddot{x_{5d}}\end{aligned} \tag{29}$$

where,

$$\begin{aligned}y = &M_{31}M_{23}M_{12} - M_{21}M_{33}M_{12} + M_{21}M_{13}M_{32} \\ &+ M_{11}M_{22}M_{33} - M_{11}M_{32}M_{23} \\ &+ M_{13}M_{31}M_{22}\end{aligned} \tag{30}$$

The dynamic equation of the Marco variable $\sigma$ is described as

$$\sigma_1 = ce_1 + \dot{e_1} \tag{31}$$

$$\sigma_2 = ce_2 + \dot{e_2} \tag{32}$$

$$\sigma_3 = ce_3 + \dot{e_3} \tag{33}$$

In this context, the scalar design for synergetic control is denoted as *c*, where *c* is a positive value.

$$\dot{\sigma_1} = c\dot{e_1} + \ddot{e_1} \tag{34}$$

$$\dot{\sigma_2} = c\dot{e_2} + \ddot{e_2} \tag{35}$$

$$\dot{\sigma_3} = c\dot{e_3} + \ddot{e_3} \tag{36}$$

The symbol $\dot{\sigma_1}$, $\dot{\sigma_2}$ and $\dot{\sigma_3}$ denote the manifold equation variable as defined within the context.

$$T\dot{\sigma_1} + \sigma_1 = 0 \tag{37}$$

$$T\dot{\sigma_2} + \sigma_2 = 0 \tag{38}$$

$$T\dot{\sigma_3} + \sigma_3 = 0 \tag{39}$$

where, $T$ is greater than 0, is the converging ratio of $\sigma$ to manifold with $\dot{\sigma}$.

By substituting Eqs. (34)-(36) into Eqs. (37)-(39), to obtain:

$$T(c\dot{e_1} + \ddot{e_1}) + \sigma_1 = 0 \tag{40}$$

$$T(c\dot{e_2} + \ddot{e_2}) + \sigma_2 = 0 \tag{41}$$

$$T(c\dot{e_3} + \ddot{e_3}) + \sigma_3 = 0 \tag{42}$$

Additionally, by utilizing Eqs. (40)-(42), one can derive:

$$\begin{aligned}T\Big(c\dot{e_1} + \Big(\tfrac{1}{y}[&(M_{22}M_{33} - M_{32}M_{23})u_1 + (M_{32}M_{13} - \\ &M_{12}M_{33})u_2 + (M_{12}M_{23} - M_{22}M_{13})u_3 + (M_{32}M_{23} - \\ &M_{22}M_{33})C_1 + (M_{32}M_{23} - M_{22}M_{33})G_1 + (M_{12}M_{33} - \\ &M_{13}M_{33})C_2 + (M_{12}M_{33} - M_{13}M_{32})G_2 + (M_{22}M_{13} - \\ &M_{12}M_{23})C_3 + (M_{22}M_{13} - M_{12}M_{23})G_3] - \ddot{x_{1d}}\Big)\Big) + \\ &\sigma_1 = 0\end{aligned} \tag{43}$$

$$\begin{aligned}T\Big(c\dot{e_2} + \Big(\tfrac{1}{y}[&(M_{31}M_{23} - M_{21}M_{33})u_1 + (M_{11}M_{33} - \\ &M_{13}M_{31})u_2 + (M_{13}M_{23} - M_{11}M_{23})u_3 + \\ &(M_{21}M_{33} - M_{31}M_{23})C_1 + (M_{21}M_{33} - M_{31}M_{23})G_1 + \\ &(M_{13}M_{31} - M_{11}M_{33})C_2 + (M_{13}M_{31} - M_{11}M_{33})G_2 + \\ &(M_{11}M_{23} - M_{21}M_{13})C_3 + (M_{11}M_{23} - \\ &M_{21}M_{13})G_3] - \ddot{x_{3d}}\Big)\Big) + \sigma_2 = 0\end{aligned} \tag{44}$$

$$\begin{aligned}T\Big(c\dot{e_3} + \Big(\tfrac{1}{y}[&(M_{32}M_{21} - M_{31}M_{22})u_1 + (M_{31}M_{12} - \\ &M_{32}M_{11})u_2 + (M_{11}M_{22} - M_{21}M_{12})u_3 + \\ &(M_{31}M_{22} - M_{32}M_{21})C_1 + (M_{31}M_{22} - M_{32}M_{21})G_1 + \\ &(M_{32}M_{11} - M_{31}M_{12})C_2 + (M_{32}M_{11} - M_{31}M_{12})G_2 +\end{aligned} \tag{45}$$

$$(M_{21}M_{12} - M_{11}M_{22})C_3 + (M_{21}M_{12} - M_{11}M_{22})G_3] - \ddot{x}_{5d}\Big)\Big) + \sigma_3 = 0$$

The synergetic control law for a prosthetic finger system can be derived from Eqs. (43)-(45), as demonstrated below:

$$u_1 = M_{11}\left(-c\dot{e}_1 + \ddot{x}_{1d} - \frac{\sigma_1}{T}\right) + M_{12}\dot{x}_4 + M_{13}\dot{x}_6 + C_1x_2 + G_1 \quad (46)$$

$$u_2 = M_{21}\dot{x}_2 + M_{22}\left(-c\dot{e}_2 + \ddot{x}_{3d} - \frac{\sigma_2}{T}\right) + M_{23}\dot{x}_6 + C_2x_4 + G_2 \quad (47)$$

$$u_3 = M_{31}\dot{x}_2 + M_{32}\dot{x}_4 + M_{33}\left(-c\dot{e}_3 + \ddot{x}_{5d} - \frac{\sigma_3}{T}\right) + C_3x_6 + G_3 \quad (48)$$

Figure 3 illustrates the schematic representation of the CSC design for a robot arm.

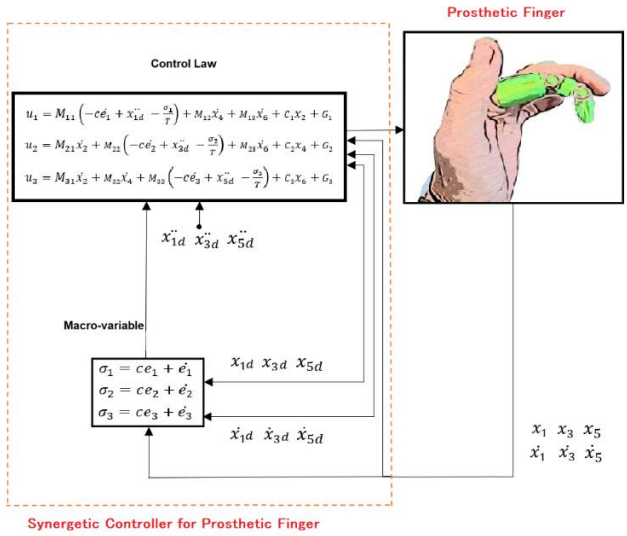


**Figure 3.** Schematic diagram of CSC

## 4. SIMULATION RESULTS AND DISCUSSION

In this work, MATLAB/SIMULINK was utilized to create and simulate a model of the prosthetic finger system. The control algorithms and system model were coded using m-functions, with the main system body designed within the SIMULINK environment. The design parameter values for the comprehensive CSC are provided in Table 1, along with configuration options for the prosthetic finger system. The CSC design parameter values for conventional CSC. The numerical design and convergence ratio were determined through a trial and error process to adjust the conventional CSC design parameters for the phalange to C and T, where their values were 1.5, and 0.00005, respectively.

**Table 1.** Design parameters of a value for a prosthetic finger system [22]

| Parameter | Definition | Value | Units |
|---|---|---|---|
| $l_1$ | Length of phalange 1 | 0.040 | m |
| $l_2$ | Length of phalange 2 | 0.025 | m |
| $l_3$ | Length of phalange 3 | 0.015 | m |
| $m_1$ | Mass of phalange 1 | 0.009 | Kg |
| $m_2$ | Mass of phalange 2 | 0.005 | Kg |
| $m_3$ | Mass of phalange 3 | 0.004 | Kg |
| $\theta_{1d}$ | Desired angle position for phalange 1 | $\frac{\pi}{2}[1 - e^{(-5t)}(5t + 1)]$ | rad |
| $\theta_{2d}$ | Desired angle position for phalange 2 | | |
| $\theta_{3d}$ | Desired angle position for phalange 3 | | |
| $g$ | Gravitational constant | 9.81 | m/s$^2$ |

## 5. VALIDATION AND VERIFICATION

To validate the results of the methodology used in this study, a comparison will be made with the reference [22], as this study is closer to the system used in this work in terms of dynamic analysis, but differs in the approach used, employing CSMC on the prosthetic finger. Therefore, the comparison will be conducted to ensure the accuracy of the algorithms used in this study.

Figure 4 illustrates the angular position results of the prosthetic finger compared with the reference [22]. Through Figure 4, it is evident that classical synergetic control has proven its efficiency and superior strength over CSMC, where observed a significant improvement in tracking angular position smoothly, without chatter, and in slightly less time than the CSMC algorithm.

Figure 5 demonstrates the arrangement of phalanx for the model controlled in CSC. It was observed that the tracking response, achieving the desired position, occurred within a maximum of 9 sec for CSC, the time taken to connect to the desired position is favorable compared to the previous study.it is intelligible that the CSC controller was able to successfully track the desired position for each phalange and stabilize, and distinguished by their efficiency, flexibility, and smoothness in terms of performance.

Figure 6 illustrates the control action of a CSC, where respectively the first, second and third phalanx control action reaches peaks were 1.559 N/m, 0.542 N/m and 0.014 N/m, and they stabilize simultaneously at 1.5 sec and demonstrated monotonous and smooth control signal behaviors for CSC controller. This behavior has enhanced the use of this type of control in various applications. It was observed that the applied torque is zero in the steady state for each controller.

Figure 7 shows the angular velocity for CSC. The first, second and third angular velocities peak at 2.354 and stabilize at 5.1 sec.

The simulation results can be seen in Figure 8 for the tracking error the CSC prosthetic finger system.

The velocity error behavior for CSC is shown in Figure 9 the system can be describing was global asymptotic stability

to the by the convergence the of angular position to each phalange to the desired position. This controller CSC can make the prosthetic finger asymptotically stable by forcing the error and the derivative of the error to reach zero at a good time in the final trajectory, resulting in precise tracking of the movement of the prosthetic finger.

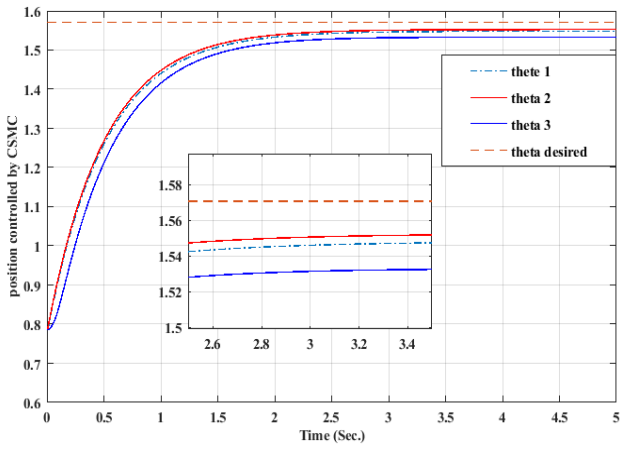


(a) CSMC

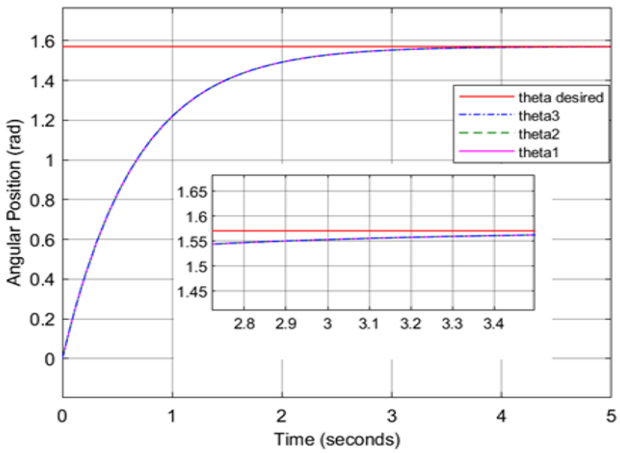


(b) CSC

**Figure 4.** Tracking performance between the desired and existing position

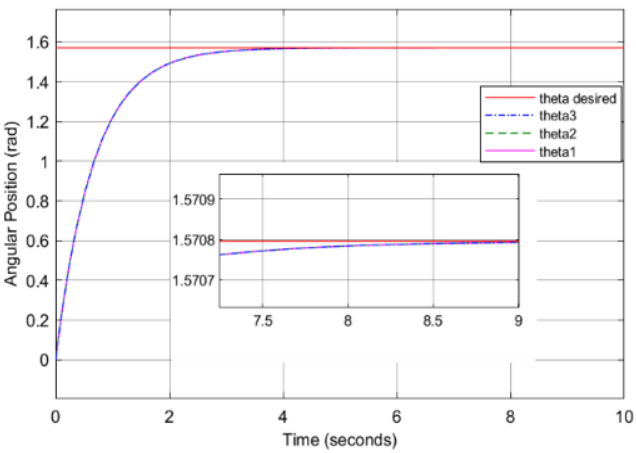


**Figure 5.** Tracking performance between the desired and existing position of CSC algorithm

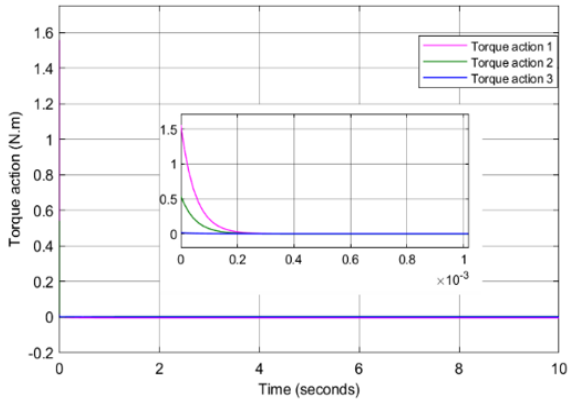


**Figure 6.** Control action response using CSC algorithm to the prosthetic finger

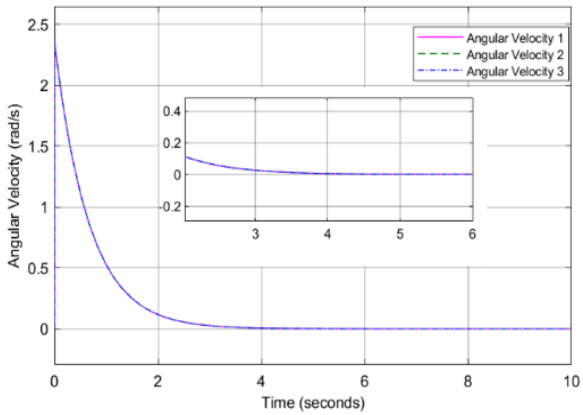


**Figure 7.** Angular velocity response for using CSC

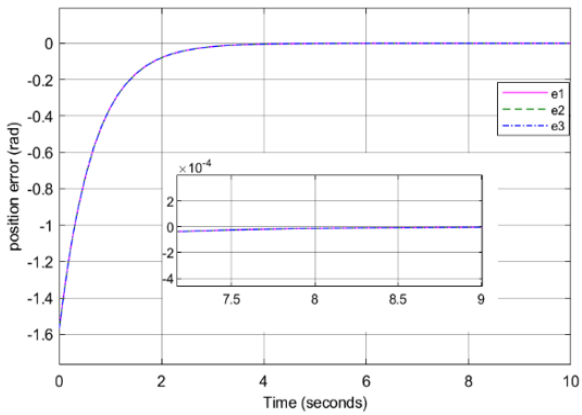


**Figure 8.** Position error response for CSC

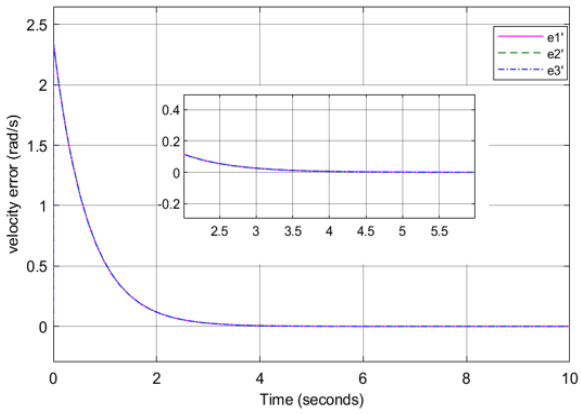


**Figure 9.** Velocity error response for CSC

## 6. UNCERTAINTY IN THE SYSTEM

During the operation of a prosthetic finger, changes in the fingertip's posture can alter the load moment of inertia on the joints. Additionally, the long driving chain is affected by various frictional forces. These factors introduce modeling uncertainty, making it necessary to estimate this uncertainty accurately. Designing control systems in atypical conditions, a robust survey of the systems under consideration is essential. Control options should be made in consecutive order if the system's many parameters are quite uncertain.

Robustness analysis for model uncertainties is used to validate the efficacy the system response and evaluate the effectiveness the CSC controller, uncertainty will be introduced into the proposed model. In addition, trial and error will be used to adjust the load mass (m) and phalanx length (l) of the controlled prosthetic finger system by 25%, 50%, 75%, and 90% [36].

Figures 10 and 11 show the angular position and angular velocity of the phalanges under the CSC (Composite State Control) method. The four subplots (a, b, c, d) in each figure correspond to different levels of system uncertainty: 25%, 50%, 75%, and 90%, respectively.

Figure 10 shows the angular position of the prosthetic finger under all levels of uncertainty (25%, 50%, 75%, and 90%), the angular position follows the desired path closely. The differences between the actual and desired angular positions are minimal, indicating that the CSC method effectively maintains the desired position. The inset graphs provide a zoomed-in view of the system's performance around 7.5 to 9 seconds, where the system's stability and precision can be observed more clearly.

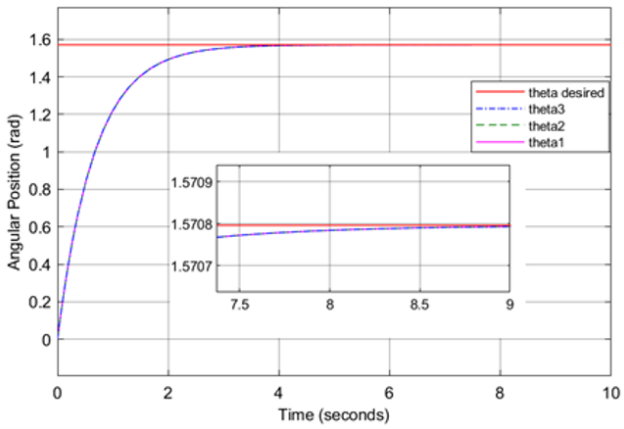


(a) 25%

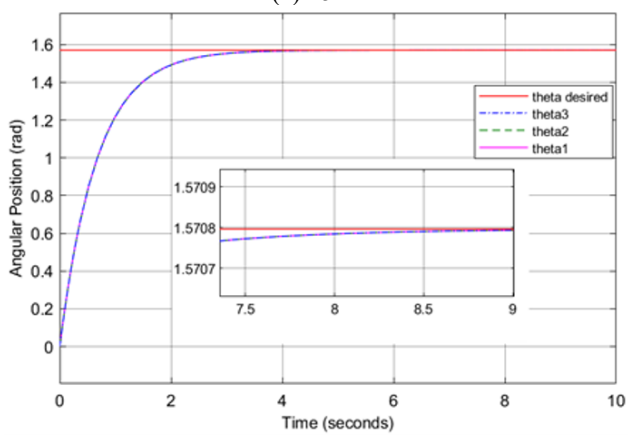


(b) 50%

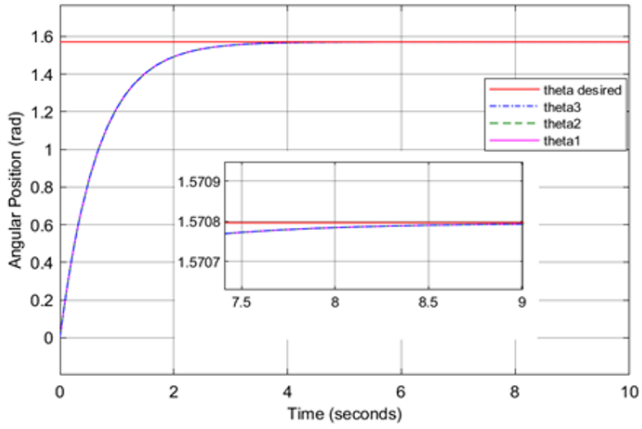


(c) 75%

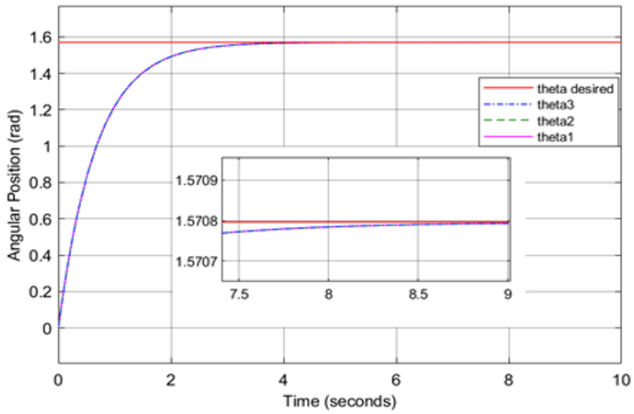


(d) 90%

**Figure 10.** Angular position function phase plot at uncertainty of CSC

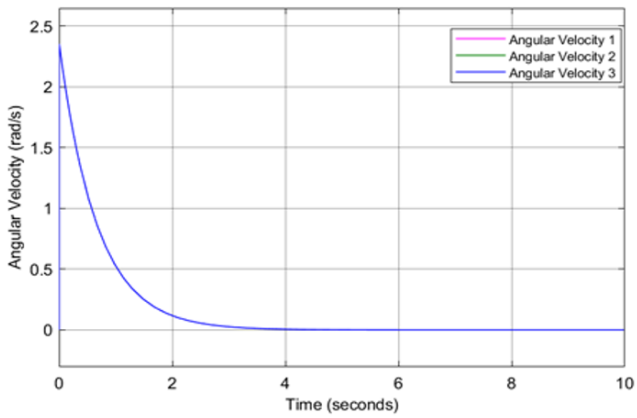


(a) 25%

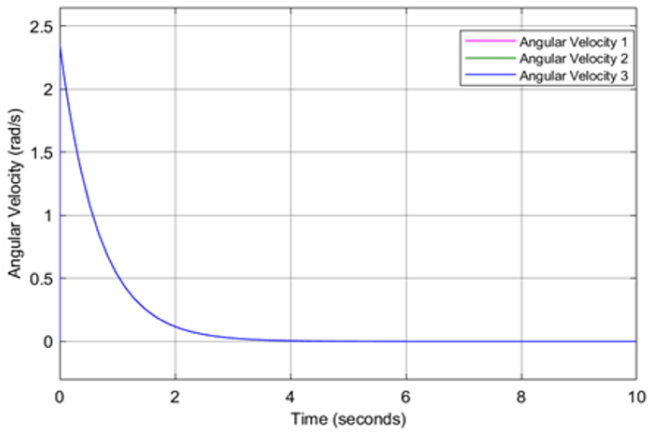


(b) 50%

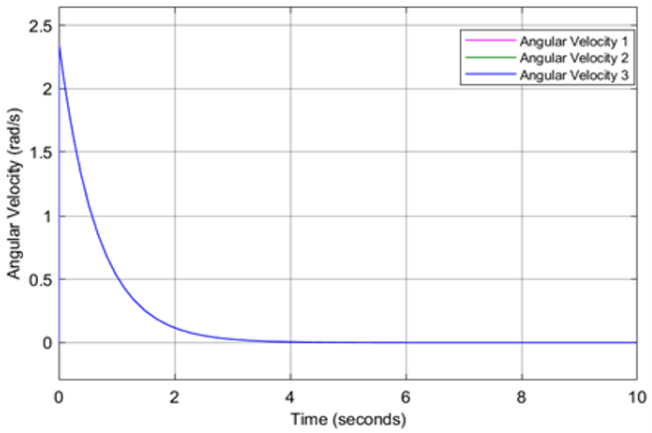


(c) 75%

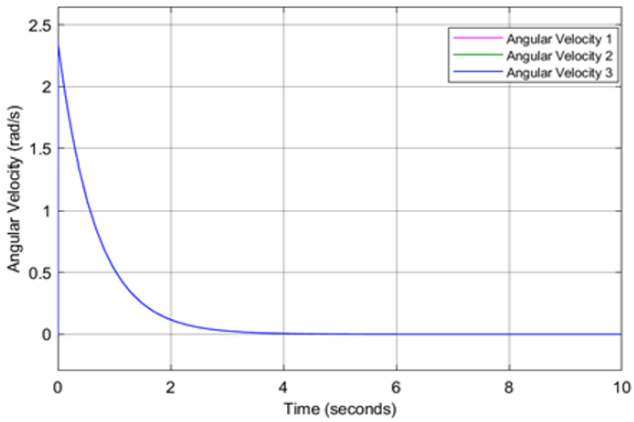


(d) 90%

**Figure 11.** Angular velocity function phase plot at uncertainty of CSC

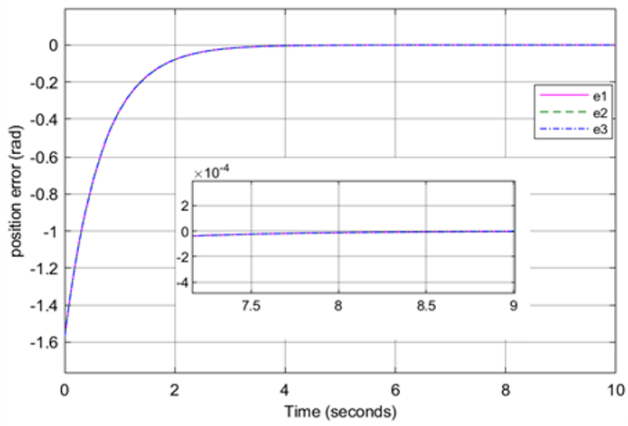


(c) 75%

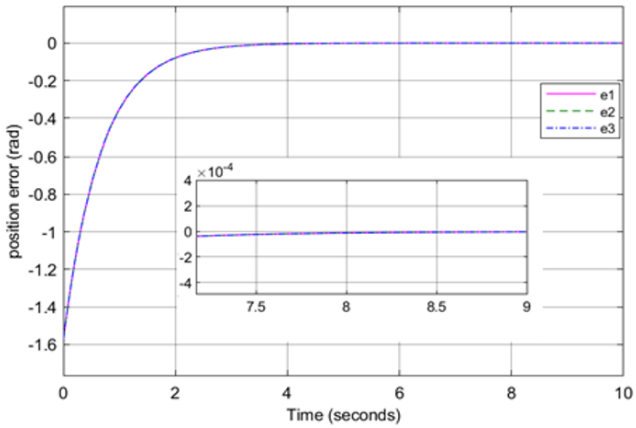


(d) 90%

**Figure 12.** Position error function phase plot at uncertainty of CSC

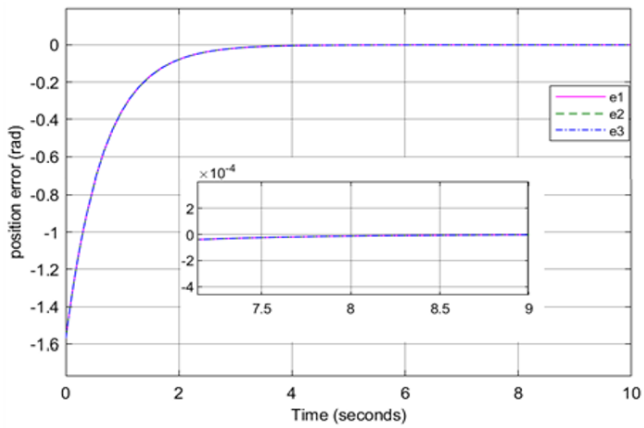


(a) 25%

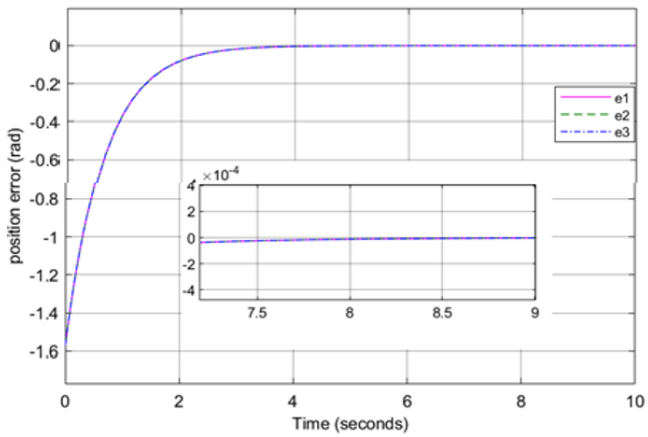


(b) 50%

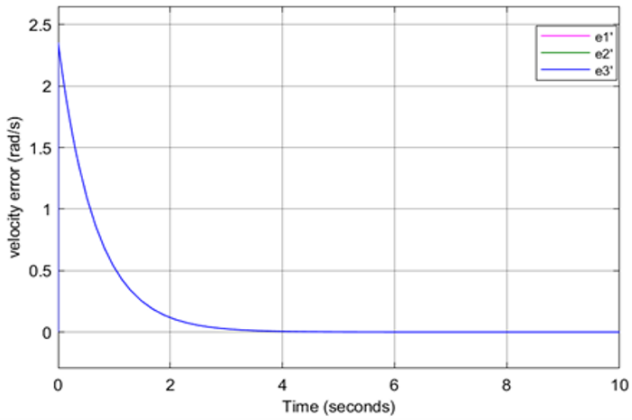


(a) 25%

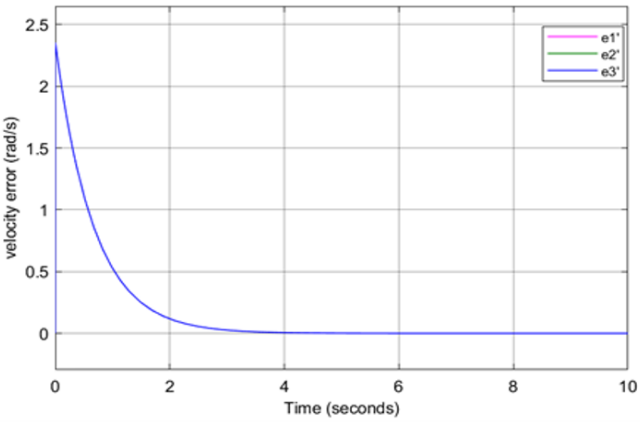


(b) 50%

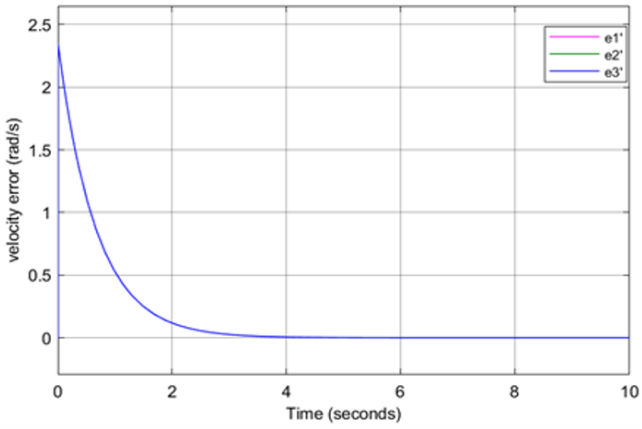


(c) 75%

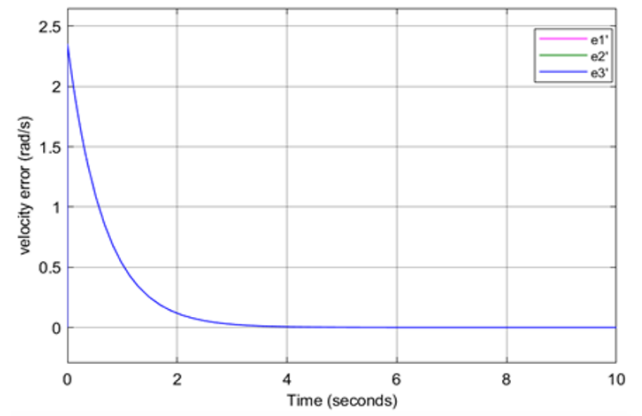


(d) 90%

**Figure 13.** Velocity error function phase plot at uncertainty of CSC

Also, the angular velocity in Figure 10, found that the angular velocity shows similar behavior across all levels of uncertainty. Wherefrom, the CSC method ensures that the velocity remains consistent with the desired trajectory. Where minimal chattering is observed, indicating a stable and robust control performance.

From the results, it is clear that the CSC method is effective in maintaining the desired angular position and velocity of the prosthetic finger even in the presence of significant uncertainty. Where the controller's performance is consistent across different levels of uncertainty, with no substantial impact on operating speed or stability duration. Therefore, this robustness suggests that the CSC method is highly reliable for controlling prosthetic devices, ensuring accurate and stable operation despite potential variations in system parameters.

Figures 12 and 13 illustrate the position and velocity error behaviors of the system under CSC (Composite State Control) control with different levels of system uncertainty: 25%, 50%, 75%, and 90%, respectively.

Figure 11 shows the position error with different uncertainties. At 25% uncertainty, found that the position error rapidly decreases and stabilizes around zero within the first few seconds. The inset shows minimal fluctuations, indicating high precision. Also, with 50% uncertainty, similar to 25% uncertainty, the position error quickly reduces and remains stable with negligible error. The behavior is consistent with previous uncertainty levels, with a rapid reduction in error and stable performance at 75% uncertainty. While at 90% uncertainty, even at the highest uncertainty level, it was found that the position error stabilizes quickly, maintaining the desired performance.

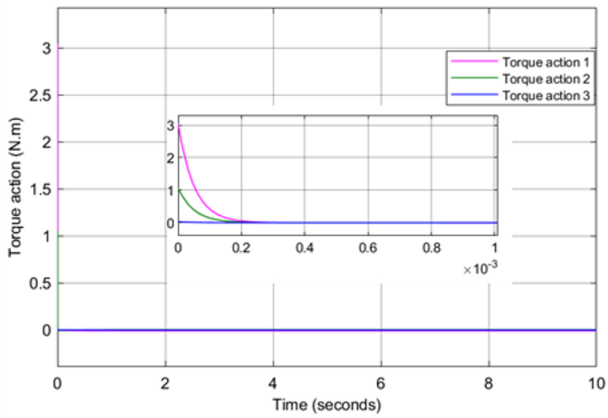


(a) 25%

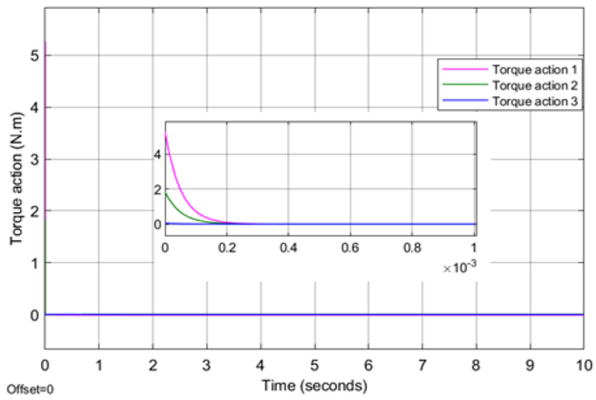


(b) 50%

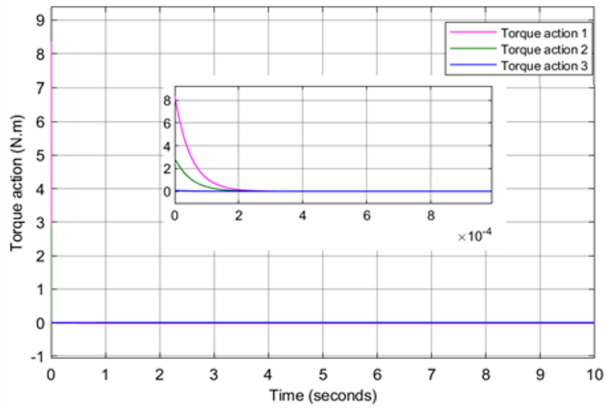


(c) 75%

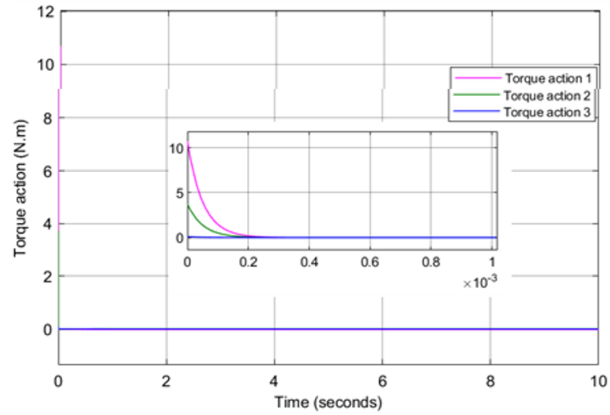


(d) 90%

**Figure 14.** Control action function phase plot at uncertainty of CSC

Figure 13 illustrates the velocity error with different uncertainties. From the figure at 25% uncertainty, found that the velocity error decreases swiftly and stabilizes close to zero. Minor fluctuations are observed in the inset. The behavior remains consistent with the previous uncertainty levels, showing rapid stabilization and minimal error at 50% uncertainty. Also, with 75% uncertainty, the velocity error follows the same trend, with fast error reduction and stable performance. While at 90% uncertainty, the velocity error still stabilizes effectively, maintaining the desired performance with minimal impact from uncertainty.

It is concluded that the CSC algorithm effectively handles position and velocity errors, even under significant uncertainty. Also, the figures show that the CSC system can maintain stability and precision regardless of parameter variations. Therefore, the minimal impact of uncertainty on the error metrics suggests that the CSC system is robust and reliable. Furthermore, this performance indicates that the CSC system is likely superior to previously used controllers, providing better stability and error management in dynamic and uncertain environments.

Figure 14 demonstrates the effect of control actions on the torque exerted on a prosthetic finger under different levels of uncertainty. Figure 14 illustrates the control actions on the torque exerted on a prosthetic finger. At 25% uncertainty, found that the torque values are relatively low, with minimal fluctuations after the initial spike. This suggests that a low level of uncertainty has a modest impact on the torque exerted on the prosthetic finger. Also, the torque values increase slightly more compared to 25% uncertainty. The initial spike is more pronounced, indicating a greater effect of uncertainty on the torque exerted, at was 50% uncertainty. Also, with 75% uncertainty, found that the torque values are significantly higher than the previous two cases. The initial spike is even more pronounced, suggesting that the control system is compensating more aggressively for the increased uncertainty. While at 90% uncertainty, the torque values are the highest among all the cases. Where is the control system responds with a substantial initial spike, indicating a high level of compensation required to manage the uncertainty.

From this it is concluded that when uncertainty increases, the torque exerted by the control system on the prosthetic finger also increases. Where this is evident from the progressive rise in the initial torque spikes across the subfigures. Also, the increase in torque values at different levels of uncertainty demonstrates the control system's adaptive response to maintain the desired performance of the prosthetic finger.

However, the effectiveness of CSC algorithm was the appears to effectively manage and compensate for the uncertainties applied to the torque exerted on the phalanges. Based on the above illustrations, it can be inferred that the introduction of uncertainty has no significant effect on the operating speed or stability duration of the system, thus verifying the efficiency of the CSC. It is able to maintain stability under different conditions allows prosthetic fingers to function well in dynamic settings. This adaptability is crucial for users who encounter varying levels of complexity in their daily routines, significantly improves the grip strength of prosthetic fingers. This means that users can perform daily tasks such as grasping objects, typing, etc. Which boosts their independence and confidence.

The findings from this research pave the way for future innovations. By integrating CSC with advanced technologies such as artificial intelligence and adaptive control.

Figure 15 shows the details these torque values, showing the numerical impact of uncertainty on the control actions. It was found that the figures clearly show that as uncertainty in the system increases, the torque exerted on the prosthetic finger also increases to compensate for this uncertainty. This relationship highlights the effectiveness of the control system in adapting to varying conditions to ensure the proper functioning of the prosthetic device.

Where is this analysis underscores the importance of robust control algorithms like CSC in managing uncertainties in prosthetic devices, ensuring their reliability and effectiveness in real-world applications.

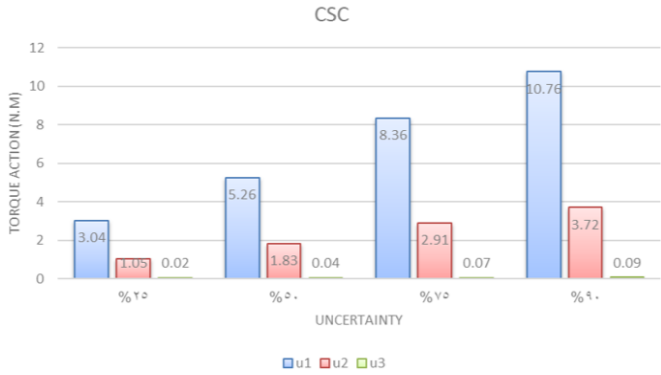


**Figure 15.** Turque action value of CSC for the prosthetic finger system

## 7. CONCLUSIONS

In this study, a synergetic control design was developed for a 3-DoF prosthetic finger system to address model uncertainty. Compared to classical sliding mode control, this synergetic control (CSC) improved performance by about 20%. Numerical simulations with varying parameters (25%, 50%, 75%, and 90%) demonstrated that the synergetic control design effectively guides the system to its desired position without oscillations, even under large parameter variations. Additionally, CSC ensures smooth and consistent control signals and prevents chattering, overcoming previous challenges in controlling nonlinear and angular motion in prosthetic fingers. The future work in this research will focus on determining the values of the CSC control parameters using one of the optimization methods. In addition to the potential for scaling to more complex robotic systems, and the challenges of real-world implementation.

Finally, CSC has proven to be a dependable and effective strategy for improving the performance and robustness of prosthetic finger systems, paving the way for future advances in precision control technology.

## REFERENCES

[1] Arefeen, A., Quarnstrom, J., Syed, S.P.Q., Bai, H., Xiang, Y. (2023). Human–robot collaborative lifting motion prediction and experimental validation. Journal of Intelligent & Robotic Systems, 109(4): 80. https://doi.org/10.1007/s10846-023-02013-y

[2] Arslan, Y.Z., Hacioglu, Y., Taskin, Y., Yagiz, N. (2015). Control of a biomimetic robot hand finger: Classical,

robust, and intelligent approaches. In Handbook of Research on Advancements in Robotics and Mechatronics, pp. 475-499. https://doi.org/10.4018/978-1-4666-7387-8.ch016

[3] Bundhoo, V., Park, E.J. (2005). Design of an artificial muscle actuated finger towards biomimetic prosthetic hands. In ICAR'05. Proceedings, 12th International Conference on Advanced Robotics, Seattle, WA, USA, pp. 368-375. https://doi.org/10.1109/ICAR.2005.1507437

[4] Arslan, Y.Z., Hacioglu, Y., Yagiz, N. (2008). Prosthetic hand finger control using fuzzy sliding modes. Journal of Intelligent and Robotic Systems, 52: 121-138. https://doi.org/10.1007/s10846-008-9207-8

[5] Zhu, J., Hao, G. (2024). Modelling of a general lumped-compliance beam for compliant mechanisms. International Journal of Mechanical Sciences, 263: 108779. https://doi.org/10.1016/j.ijmecsci.2023.108779

[6] Pertuz, S.A., Peña, C.A., Riaño, C.I. (2023). Design and building of a multi-finger robotic hand prototype for grip control. International Journal of Mechanical Engineering and Robotics Research, 12(5): 264-274. https://doi.org/10.18178/ijmerr.12.5.264-274

[7] Espinosa Garcia, F.J., Lugo-González, E., Telléz-Velázquez, A., Arias-Montiel, M., Ceccarelli, M. (2022). Optimal position fuzzy control of an underactuated robotic finger. Mathematical Problems in Engineering, 2022(1): 2091337. https://doi.org/10.1155/2022/2091337

[8] Xu, K., Zhao, J., Du, Y., Sheng, X., Zhu, X. (2013). Design and postural synergy synthesis of a prosthetic hand for a manipulation task. In 2013 IEEE/ASME International Conference on Advanced Intelligent Mechatronics, Wollongong, NSW, Australia, pp. 56-62. https://doi.org/10.1109/AIM.2013.6584068

[9] Lysenko, A., Khashev, D., Uryanskaya, E. (2017). Development of a mathematical model of a biomechatronic finger prosthesis as part of a multifunctional prosthetic hand. MATEC Web of Conferences, 132: 02003. https://doi.org/10.1051/matecconf/201713202003

[10] Humaidi, A.J., Ibraheem, I.K., Azar, A.T., Sadiq, M.E. (2020). A new adaptive synergetic control design for single link robot arm actuated by pneumatic muscles. Entropy, 22(7): 723. https://doi.org/10.3390/e22070723

[11] Al-Hussein, A.B.A., Tahir, F.R., Ouannas, A., Sun, T.C., Jahanshahi, H., Aly, A.A. (2021). Chaos suppressing in a three-buses power system using an adaptive synergetic control method. Electronics, 10(13): 1532. https://doi.org/10.3390/electronics10131532

[12] Shadow Robot. (2021). Shadow dexterous hand technical specification. https://www.shadowrobot.com/wp-content/uploads/2022/03/shadow_dexterous_hand_e_technical_specification.pdf.

[13] Fan, S., Gu, H., Zhang, Y., Jin, M., Liu, H. (2018). Research on adaptive grasping with object pose uncertainty by multi-fingered robot hand. International Journal of Advanced Robotic Systems, 15(2). https://doi.org/10.1177/1729881418766783

[14] Li, X., Chen, Z., Ma, C. (2021). Optimal grasp force for robotic grasping and in-hand manipulation with impedance control. Assembly Automation, 41(2): 208-220. https://doi.org/10.1108/AA-11-2020-0180

[15] Shahriari, E., Birjandi, S.A.B., Haddadin, S. (2022). Passivity-based adaptive force-impedance control for modular multi-manual object manipulation. IEEE Robotics and Automation Letters, 7(2): 2194-2201. https://doi.org/10.1109/LRA.2022.3142903

[16] Zhang, T., Jiang, L., Fan, S., Wu, X., Feng, W. (2016). Development and experimental evaluation of multi-fingered robot hand with adaptive impedance control for unknown environment grasping. Robotica, 34(5): 1168-1185. https://doi.org/10.1017/S0263574714002161

[17] Jalani, J., Mahyuddin, N., Herrmann, G., Melhuish, C. (2013). Active robot hand compliance using operational space and integral sliding mode control. In 2013 IEEE/ASME International Conference on Advanced Intelligent Mechatronics, Wollongong, NSW, Australia, pp. 1749-1754. https://doi.org/10.1109/AIM.2013.6584350

[18] Herrmann, G., Jalani, J., Mahyuddin, M.N., Khan, S.G., Melhuish, C. (2016). Robotic hand posture and compliant grasping control using operational space and integral sliding mode control. Robotica, 34(10): 2163-2185. https://doi.org/10.1017/S0263574714002811

[19] Labbadi, M., Cherkaoui, M. (2019). Robust adaptive backstepping fast terminal sliding mode controller for uncertain quadrotor UAV. Aerospace Science and Technology, 93: 105306. https://doi.org/10.1016/j.ast.2019.105306

[20] Mohd Zaihidee, F., Mekhilef, S., Mubin, M. (2019). Robust speed control of PMSM using sliding mode control (SMC)—A review. Energies, 12(9): 1669. https://doi.org/10.3390/en12091669

[21] Jung, S. (2018). Improvement of tracking control of a sliding mode controller for robot manipulators by a neural network. International Journal of Control, Automation and Systems, 16(2): 937-943. https://doi.org/10.1007/s12555-017-0186-z

[22] Majeed, H.S., Kadhim, S.K., Jaber, A.A. (2022). Design of a sliding mode controller for a prosthetic human hand's finger. Engineering and Technology Journal, 40(1): 257-266. http://doi.org/10.30684/etj.v40i1.1943

[23] Ajwad, S.A., Islam, R.U., Azam, M.R., Ullah, M.I., Iqbal, J. (2016). Sliding mode control of rigid-link anthropomorphic robotic arm. In 2016 2nd International Conference on Robotics and Artificial Intelligence (ICRAI), Rawalpindi, Pakistan, pp. 75-80. https://doi.org/10.1109/ICRAI.2016.7791232

[24] Yagiz, N., Arslan, Y.Z., Hacioglu, Y. (2007). Sliding mode control of a finger for a prosthetic hand. Journal of Vibration and Control, 13(6): 733-749. https://doi.org/10.1177/1077546307072352

[25] Jones, G.K., Stopforth, R. (2016). Mechanical design and development of the touch hand ii prosthetic hand. R&D Journal, 32: 23-34.

[26] Mohammed, R.A., Abd Soud, W., Baqer, I.A. (2021). Kinematic analysis of underactuated robotic finger design. IOP Conference Series: Materials Science and Engineering, 1094(1): 012070. https://doi.org/10.1088/1757-899X/1094/1/012070

[27] Baccouch, M., Dodds, S. (2020). A two-link robot manipulator: Simulation and control design. International Journal of Robotic Engineering, 5(12): 2-17. https://doi.org/10.35840/2631-5106/4128

[28] Ali, S.S., Raafat, S.M., Al-Khazraji, A. (2020). Improving the performance of medical robotic system

using $H_\infty$ loop shaping robust controller. International Journal of Modelling, Identification and Control, 34(1): 3-12. https://doi.org/10.1504/IJMIC.2020.108911

[29] Ahmed, A.S., Kadhim, S.K. (2023). Non-leaner control on the pneumatic artificial muscles: A comparative study between adaptive backstepping and conventional backstepping algorithms. Mathematical Modelling of Engineering Problems, 10(2): 653-662. https://doi.org/10.18280/mmep.100236

[30] Ahmed, A.S., Kadhim, S.K. (2022). A comparative study between convolution and optimal backstepping controller for single arm pneumatic artificial muscles. Journal of Robotics and Control (JRC), 3(6): 769-778. https://doi.org/10.18196/jrc.v3i6.16064

[31] Shanan, D.S., Kadhim, S.K. (2023). Comparative analysis of airflow regulation in ventilator systems using various control strategies. Journal Européen des Systèmes Automatisés, 56(5): 811-821. https://doi.org/10.18280/jesa.560512

[32] Benbouhenni, H. (2021). Synergetic control theory scheme for asynchronous generator based dual-rotor wind power. Journal of Electrical Engineering, Electronics, Control and Computer Science, 7(3): 19-28.

[33] Essiane, S.N., Bissé, J.T., Pesdjock, M.J.P. (2020). Simple adaptive synergetic control scheme based on the MIT rule of the DC motor. European Journal of Applied Physics, 2(6). https://doi.org/10.24018/ejphysics.2020.2.6.30

[34] Mahdi, S.M., Yousif, N.Q., Oglah, A.A., Sadiq, M.E., Humaidi, A.J., Azar, A.T. (2022). Adaptive synergetic motion control for wearable knee-assistive system: A rehabilitation of disabled patients. Actuators, 11(7): 176. https://doi.org/10.3390/act11070176

[35] Sheltag, D., Kadhim, S.K. (2024). Enhancing artificial ventilator systems: A comparative analysis of traditional and nonlinear PID controllers. Mathematical Modelling of Engineering Problems, 11(3): 599-610. https://doi.org/10.18280/mmep.110303

[36] Salman, M.A., Kadhim, S.K. (2022). Optimal backstepping controller design for prosthetic knee joint. Journal Européen des Systèmes Automatisés, 55(1): 49-59. https://doi.org/10.18280/jesa.550105